Geosci. Model Dev. Discuss., 2, 681–707, 2009
www.geosci-model-dev-discuss.net/2/681/2009/

Geoscientific
Model Development
Discussions

Geoscientific Model Development Discussions is the access reviewed discussion forum of *Geoscientific Model Development*

Implementation of a new aerosol HAM model within the Weather Research and Forecasting (WRF) modeling system

R. Mashayekhi[1,2], **P. Irannejad**[1], **J. Feichter**[2], **and A. A. Bidokhti**[1]

[1]Institute of Geophysics, University of Tehran, Tehran, Iran
[2]Max Planck Institute for Meteorology, Hamburg, Germany

Received: 23 May 2009 – Accepted: 4 June 2009 – Published: 1 July 2009

Correspondence to: R. Mashayekhi (rmash@ut.ac.ir)

Published by Copernicus Publications on behalf of the European Geosciences Union.

Abstract

A new coupled system of aerosol HAM model and the Weather, Research and Forecasting (WRF) model is presented in this paper. Unlike the current aerosol schemes used in WRF model, the HAM is using a "pseudomodal" approach for the representation of the particle size distribution. The aerosol components considered are sulfate, black carbon, particulate organic matter, sea salt and mineral dust. The preliminary model results are presented for two different 6-day simulation periods from 22 to 28 February 2006 as a winter period and 6 to 12 May 2006 as a mild period. The mean shortwave radiation and thermal forcing were calculated from the model simulations with and without aerosols feedback for two simulation periods. A negative radiative forcing and cooling of the atmosphere were found mainly over the regions of high emission of mineral dust. The absorption of shortwave radiation by black carbon caused warming effects in some regions with positive radiative forcing. The simulated daily mean sulfate mass concentration showed a rather good agreement with the measurements in the European EMEP network. The diurnal variation of the simulated hourly PM_{10} mass concentration at Tehran was also qualitatively close to the observations in both simulation periods. The model captured diurnal cycle and the magnitude of the observed PM_{10} concentration during most of the simulation periods. The differences between the observed and simulated PM_{10} concentration resulted mostly from limitation of the model in simulating the clouds and precipitation, transport errors and uncertainties in the particulate emission rates. The inclusion of aerosols feedback in shortwave radiation scheme improved the simulated daily mean shortwave radiation fluxes in Tehran for both simulation periods.

GMDD

2, 681–707, 2009

1 Introduction

Aerosol particles suspended in the Earth's atmosphere are an important component of the present day climate system. These submicron particles from both natural and anthropogenic sources affect the Earth's radiative balance directly by scattering (Charlson et al., 1992) or absorbing (Ramanathan and Vogelmann, 1997) solar radiation. Furthermore, aerosol particles modify the cloud properties by acting as cloud condensation nuclei (CCN), thereby influencing the albedo (Twomey, 1991; Charlson et al., 1987), lifetime (Albrecht, 1989), extent and precipitation (Ramanathan et al., 2001a, b) of clouds.

Throughout the last decade several aerosol modules were developed to improve the characterization of concentration, size distribution and composition of aerosols. Methods used to represent aerosol size distributions have been reviewed in detail by Williams and Loyalka (1991) and Whitby and McMurry (1997). In recent years, several studies have included predictions of explicit size distributions of internal mixtures. Sectional models have been used in multicomponent 3-D studies (e.g. Jacobson, 2001; Gong et al., 2003; Rodriguez and Dabdub, 2004). Modal models have also been employed in regional-scale air quality models (e.g. Ackermann et al., 1998; Schell et al., 2001) offering computational advantages over the sectional approach.

Despite numerous studies, the level of understanding of the aerosol effects on climate change is still very low (IPCC, 2007). Realistic simulation of the radiative effects of aerosols requires models where the aerosols, meteorology, radiation, and chemistry are coupled in a fully interactive manner. The design of the community Weather Research and Forecasting/Chemistry (WRF-Chem) prediction model (Grell et al., 2005) permits such interactive coupling. The modular framework of WRF permits it to be used for research purposes so that different aerosol modules can be evaluated and compared using the same emissions and meteorology.

Over the last few years, various aerosol modules have been implemented into the chemistry version of WRF (Ackermann et al., 1998; Schell et al., 2001; Zaveri et

GMDD
2, 681–707, 2009

al., 2005a, b). In this study, the new aerosol HAM module developed by Stier et al. (2005) has been coupled with the WRF-Chem modeling system and tested by comparison to measurements. Embedded in the ECHAM5 general circulation model, the aerosol model HAM predicts the evolution of an ensemble of microphysically interacting internally- and externally-mixed aerosol populations. A "pseudomodal" approach is used for the representation of aerosol size distributions in HAM. The major global aerosol compounds such as sulfate, black carbon, particulate organic matter, sea salt and mineral dust are included in our coupled system.

Section 2 describes the processes considered in the current coupled system. The preliminary model results for two different 6-day simulation periods in February and May 2006 are presented in Sect. 5. Finally, Sect. 6 concludes the discussion and presents an outlook to future developments.

2 Model description

The chemistry version of the Weather Research and Forecasting model (WRF-Chem) version 2.1.2 formed the starting point for the model used in this study. A full description of WRF-Chem can be found in Grell et al. (2005). Only a brief description of the major processes considered in our new coupled system, is presented here.

2.1 Size distribution

The aerosol population in HAM is represented by superposition of seven modes (Table 1), assuming a lognormal distribution within each mode:

$$n(\ln r) = \sum_{i=1}^{7} \frac{N_i}{\sqrt{2\pi}\ln\sigma_i} \exp\left(\frac{-(\ln r - \ln \bar{r}_i)^2}{2\ln^2\sigma_i}\right) \quad (1)$$

where N_i is the number of aerosols, r is the particle diameter, $\bar{r}$ is the number median radius, and σ is the standard deviation of the distribution mode i. The standard devi-

GMDD
2, 681–707, 2009

ation is assumed to be constant and set to σ=1.59 μm for the nucleation, Aitken and accumulation modes and to σ=2.00 μm for the coarse size mode (Wilson et al., 2001).

The seven modes are grouped into four geometrical size classes, ranging from the nucleation, Aitken and accumulation modes to coarse mode. Besides size, two types of particles are distinguished, internally mixed and water soluble particles (four modes), and externally mixed and insoluble particles (three modes). The separation of the aerosol population into these two populations allows predicting the hygroscopic properties of initially insoluble compounds, which controls their atmospheric lifetimes and also their interaction with clouds. The modal setup and the underlying mixing concept are illustrated in Table 1. The evolution of size distributions of most of the key components of the global aerosol burden including sulfate, black and primary organic carbon, sea salt and mineral dust has been considered in this study. Three of the modes constitute solely of insoluble compounds; four of the modes contain at least one soluble compound.

2.2 Aerosol microphysics module

The microphysics core of HAM is based on the aerosol module M7 (Vignati et al., 2004) which itself is a development of the earlier version M3+ regarding the physics and dynamics involved. The full description of M7 can be found in Vignati et al. (2004). M7 considers coagulation, condensation on pre-existing aerosols, aerosol nucleation, thermodynamical equilibrium with water vapor, and the inter-modal transfer.

The maximum amount of total condensable sulfate is first calculated using the available gas phase sulfate and the diffusion of the sulfate to the surface of the particles (Fuchs, 1959). Then, in the second step, the remaining gas phase sulfate is available for the nucleation of new clusters. There are two optionally available nucleation schemes in the current version of M7 following the methods suggested by Kulmala et al. (1998) and Vehkamaki et al. (2002). The number of nucleated particles as well as the integral mass of the nucleated sulfate is parameterized based on the temperature (T), relative humidity (RH), and the gas-phase concentration of the sulfate

available after the condensation. Compared to the Kulmala method, the Vehkamaki scheme has the advantage of covering an extended range of thermodynamical conditions (0.01%<RH<100%, 230.15 K<T<305.15 K) and the usage of a more stringent application of nucleation theory.

Gaseous sulfuric acid condenses on all soluble and insoluble modes in M7. The distinction between condensation on insoluble and on mixed/soluble particles is realized by the assumption of different accommodation coefficients of α=0.3 for the insoluble and α=1.0 for the soluble particles (Vignati et al., 2004). It is also assumed that the condensation of sulfate on insoluble particles transfers them to the corresponding mixed modes.

The aerosol size distributions can be also altered by particle collision and coagulation. The treatment of coagulation in M7 is represented by the effects caused by Brownian motion (Fuchs, 1964). The coagulation coefficients for particles of modes i and j is:

$$K_{ij} = \frac{16\pi\tilde{r}\tilde{D}}{\frac{4\tilde{D}}{\tilde{v}\tilde{r}} + \frac{\tilde{r}}{\tilde{r}+\tilde{\Delta}}} \quad (2)$$

where $\tilde{D}$, $\tilde{v}$ and $\tilde{\Delta}$ are respectively the diffusion coefficient, thermal velocity and mean free path length for an aerosol particle having a geometric mean radius equal to the average of those of modes i and j: $\tilde{r}=\frac{\bar{r}_i+\bar{r}_j}{2}$.

M7 allows both inter-modal and intra-modal coagulation. A particle resulting from intra-modal coagulation remains in the same mode, so that the total mass concentration of the mode remains unchanged, but as the number of particles decreases the average particle mass increases. For inter-modal coagulation, when a particle from mode i coagulates with a larger particle from mode j, the average dry mass of mode i is transferred to mode j. The transfer of number and mass is consistent, so that the average mass of the particles in mode i remains unchanged, while that of mode j increases. The inter-modal and intra-modal coagulation of insoluble accumulation mode and all coarse modes is assumed sufficiently long to be ignored in M7.

GMDD
2, 681–707, 2009

2.3 Removal mechanisms

2.3.1 Sedimentation and dry deposition

The gravitational sedimentation and dry deposition, i.e. the transport of trace gases and particles from the atmosphere to the earth's surface, are the important sinks of atmospheric trace gases and particles. In this study, the flux of trace gases and particles from the atmosphere to the surface is calculated by multiplying concentrations in the lowest model layer by the spatially and temporally varying deposition velocity.

The deposition velocity of the species is calculated using an analogy to the Ohm's law in electrical circuits. It is proportional to the sum of three characteristic resistances (aerodynamic resistance, sub-layer resistance, surface resistance). The deposition velocity $\boldsymbol{v_d}$ for each aerosol mode is given by:

$$\boldsymbol{v_d} = (r_a + \widehat{\boldsymbol{r_d}} + r_a \widehat{\boldsymbol{r_d}} \widehat{\boldsymbol{v_G}})^{-1} + \widehat{\boldsymbol{v_G}} \tag{3}$$

where r_a is the surface resistance, $\boldsymbol{r_d}$ is the quasi-laminar sub-layer resistance which has been parameterized by considering the effects of Brownian diffusivity. The third term within the brackets is related to the aerodynamic resistance and $\widehat{\boldsymbol{v_G}}$ is the settling velocity (Slinn and Slinn, 1980; Pleim et al., 1984). The method developed by Wesely (1989) is used for the parameterization of surface resistance. In this parameterization, the surface resistance is derived from the resistances of the surfaces of the soil and the plants. The properties of the plants are determined using land-use data and the season. The surface resistance also depends on the diffusion coefficient, the reactivity, and water solubility of the reactive trace gases.

2.3.2 Wet deposition

A simplified wet deposition scheme is used for scavenging of particles by precipitation. The fraction of scavenged tracers is calculated from the in-cloud content utilizing the precipitation formation rate of the WRF cloud scheme. The partitioning be-

GMDD
2, 681–707, 2009

tween interstitial and in hydrometeors incorporated particles is prescribed by a size- and composition-dependent scavenging parameter R (Stier et al., 2005). R is defined as the fraction of the tracer in the cloudy part of the grid box that is embedded in the cloud liquid/ice water. The prescribed values of R for each mode are given in Table 2.

2.4 Aerosol-radiation interactions

The aerosol chemical properties and sizes are used to determine the aerosol optical properties. The extinction coefficient, single-scattering albedo and the asymmetry factor for scattering are computed as a function of wavelength using the method outlined in Fast et al. (2006). In brief, each chemical constituent of the aerosol is associated with a real and a complex index of refraction. The overall refractive indexes for a given mean radius of the respective mode are determined by volume weighted averages, and summed up over all modes to determine composite aerosol optical properties. Particle growth by ambient relative humidity is taken into account. Once composite aerosol optical properties are known, the effect of aerosols on incoming solar radiation within WRF-Chem is determined by transferring the relevant parameters to the Goddard shortwave radiation scheme (Chou et al., 1998).

3 Configuration of the model

Two different periods between 00:00 UTC 22 February and 00:00 UTC 28 February 2006 and between 00:00 UTC 6 May and 00:00 UTC 12 May 2006 were chosen for simulation. The simulation domain of interest in this study encompasses the south-western Asia, North Africa and some parts of Europe, with a 30-km grid spacing. It covers the latitude and longitude of 16 to 57° N and 13 to 67° E, respectively.

The vertical coordinate extends up to ~16 km a.m.s.l. and includes 31 vertical levels. Table 3 lists the configuration options for the model used in this study. The initial conditions and lateral boundary conditions are obtained from the NCEP-GFS model's

6-hourly data. Horizontally homogenous initial conditions have been assumed for aerosol particles. The initial PM_{10} mass was based on values from measurements in Tehran ($20\,\mu g\,m^{-3}$ at 00:00 UTC 6 May and $12\,\mu g\,m^{-3}$ at 00:00 UTC 22 February 2006).

4 Emission rates

For all aerosol compounds in this study, the emission flux, distribution and height are based on the prescribed Emission Inventory for the Aerosol Model Inter-comparison Experiment B AEROCOM (http://nansen.ipsl.jussieu.fr/AEROCOM/) representative for the year 2000 (Dentener et al., 2006). With the exception of the sulfur compounds, all emissions are treated as primary emissions, i.e. the compounds are assumed to be emitted as particulate matter. For simplicity, a constant monthly mean emission rate is considered for each aerosol species in the present study.

5 Results and discussion

5.1 Shortwave radiation and temperature

The spatial distributions of the simulated temperature and downward shortwave radiation by the coupled WRF-HAM model are presented first. Figures 1 and 2 illustrate the simulated shortwave radiation flux and air temperature at 2 m above the surface averaged over the 6-day simulation periods in February and May, respectively. The average differences between the simulated total shortwave radiation and temperature with and without aerosols over the simulation periods are also shown in these figures.

Figure 1c indicates a considerable negative radiative forcing over regions of high emissions of mineral dust. The magnitude of negative radiative forcing by dust aerosols exceeds $20\,W\,m^{-2}$ over the deserts in North Africa. There are also regions with positive radiative forcing which is mostly due to the absorption effects of black carbon from

anthropogenic emission sources (Fig. 1c). The value of this positive radiative forcing is less than 5 W m^{-2}. Figure 1d shows the cooling effects up to 0.6°C which is produced by the mineral dust aerosols.

The simulated mean shortwave radiation and temperature and the differences between these simulated fields with and without aerosol feedbacks in May period is illustrated in Fig. 2. Figure 2c shows a rather large area of negative radiative forcing of up to 15 W m^{-2} over the regions of emission of dust. The regions with the positive radiative forcing up to 20 W m^{-2} are also seen in Fig. 2c. The magnitude of negative forcing in May is 10 W m^{-2} lower than that in February, while the positive forcing is 15 W m^{-2} higher than that in the February period. The reason is the lower loading of mineral dust and the higher emission of black carbon in May period than those in February in this study. Figure 2d shows the difference in mean simulated temperature by WRF-HAM model with and without aerosols. The dust aerosols produce a cooling effect with the maximum value of 0.6°C over the desert in Iraq. The maximum warming effect by aerosols is up to 0.5°C over the Persian Gulf due to the absorption of shortwave radiation by black carbon from fossil fuel sources in this area.

5.2 Simulation of sulfate

Figure 3 shows the simulated and observed daily averaged aerosol mass concentration for sulfate (SO_4) during the time period between 6 and 12 May 2006. The measurements used in this section were taken from the Co-operative Program for Monitoring and Evaluation of the Long-range Transmission of Air Pollutants in Europe (EMEP) (accessible online: http://www.nilu.no/projects/ccc/emepdata.html) which provides the available aerosol sulfate datasets over most parts of Europe from the EMEP monitoring network. The colored circles in this figure present the observed daily mean sulfate mass available over the EMEP sites. The simulated daily averaged sulfate mass is in rather good agreement with the measurements at most of the measurement sites, except for a few points such as in Italy, where the model underestimates seriously the sulfate mass during the first four simulation days. The bias in simulating the sulfate

mass in Italy correctly is most likely due to too low emission rates for sulfur dioxide used in the simulation.

5.3 Diurnal variation of PM_{10}

High particulate matter concentrations with an aerodynamic diameter less than 10 μm (PM_{10}) constitute a serious air quality problem in most of the arid regions of the World and also in the industrial-highly populated urban areas. In this section, the city of Tehran has been selected as a high populated and polluted city. We compared the simulated PM_{10} mass concentration (a summation over all aerosol compounds considered by the model including sulfate, black and organic carbon, sea salt and dust concentrations) with the observations in Tehran. The observed and simulated PM_{10} mass concentrations during the two different simulation periods in Tehran are shown in Fig. 4. The hourly values of PM_{10} mass, used in this study, are derived by averaging the measurements made by the Air Quality Company at three monitoring sites in Tehran. Figure 4a shows the simulated PM_{10} mass for the time period between 22 and 28 February 2006 in Tehran. The simulated variations in PM_{10} concentrations are qualitatively similar to the measurements during most of this period. The predicted daytime peak of the PM_{10} concentrations often occurred at the same day-times as the observations. The largest differences between the observations and simulations occurred on the last two days, when the simulated PM_{10} mass is higher than the observed one. The model does not reproduce all the observed fine structure of temporal PM_{10} variations.

Figure 4b compares the PM_{10} aerosol mass in Tehran with the predictions for the time period between 6 and 12 May 2006. The time variations in the predicted PM_{10} are in a rather good agreement with the measurements during most of the period. The model captures the diurnal cycle and the magnitude of the observed PM_{10} mass concentration, except for the last day of the forecast when scavenging by precipitation occurred during the afternoon of 11 May 2006. The precipitation predicted by the model for this day (1 mm) is considerably lower than the 16 mm observed.

The simulated PM_{10} concentration peaks in the early morning, when the atmosphere is stably stratified. Concentrations decrease to minimum in the mid-afternoon due to the development of thermal instability and growth of the convective boundary layer. The observations often show two maxima of PM_{10} concentration. The fist peak occurs at around midnight and subsequently decreases during the night with a minimum occurring in the late night, when emissions are significantly reduced. The second observed peak occurs in the morning when the atmosphere is rather stable and the emissions of PM_{10} mostly from traffic take place. The model did not capture the minimum of the PM_{10} concentration observed in the late night. That is expected, because we have not used the diurnally varying rate of PM_{10} emissions from the surface, but a constant rate for each aerosol throughout the simulation period. Thus, some characteristic features of the local have not been considered by the model. Another factor that might have contributed to these differences is the coarse resolution (30 km) used for the numerical experiments.

Figure 4 also shows the contribution of each aerosol compounds in PM_{10} during the two selected episodes of 14:00 LST 26 to 08:00 LST 27 February 2006 as a high PM_{10} episode and 11:00 to 18:00 LST 22 February 2006 as a low PM_{10} condition. The mineral dust is the largest contributor to the total PM_{10} mass concentration. It represents 97% of the modeled PM_{10} concentration during the selected high PM_{10} episode (Fig. 4d) and 85% during the low PM_{10} episode (Fig. 4c).

5.4 Aerosol-radiation feedback

The simulated incident shortwave radiation flux at the surface in Tehran is compared with measurements during the two simulation periods. Figure 5a and b displays the simulated diurnal cycle of the shortwave radiation flux with the measurements, respectively, during the time periods from 22 to 28 February and 6 to 12 May 2006 in Tehran.

The simulated downward shortwave radiation is during both episodes close to the measured one, except at the first and the last day of the February simulation period (Fig. 5a). For both days, the Tehran meteorological station has reported a cloudy sky,

while the model failed to simulate observed cloud cover correctly, probably because of the coarse resolution used for these runs.

Figure 6 illustrates how the inclusion of aerosols affects the daily mean simulated downward shortwave radiation for the daytime hours during the two simulation periods. The cooling effect of aerosols is clearly seen in both simulations. When aerosols are included, the simulated daily mean shortwave radiation is generally 10 to 60 $W\,m^{-2}$ closer to the observations. The largest differences between the simulated and observed shortwave radiation occurred on 27 February due to the limitation of the model in simulating cumulus clouds.

6 Conclusions and outlook

A new coupled aerosol-atmospheric circulation model including the aerosol module HAM implemented into the Weather Research and Forecasting (WRF) model is presented. The preliminary model results for two different simulation periods from 6 to 12 May and 22 to 28 February 2006 are evaluated against the available surface measurements made by the Air Quality Company in Tehran and the European EMEP network datasets. The mean shortwave radiation and temperature forcing are calculated from the model simulations with and without aerosols feedback for the two simulation periods. A negative radiative forcing and the resulting cooling effect are found mainly over the regions of high emission of mineral dust. The absorption of shortwave radiation by black carbon aerosols causes some regions with positive radiative forcing with warming effects. The magnitude of the negative radiative forcing in May period is lower than that in February, while the positive forcing is higher. This is mostly due to the higher loading of mineral dust and lower emissions of black carbon in February than those in May.

The simulated daily mean sulfate mass agreed with that observed in most of the EMEP measurement sites during the simulation period in May. The time variations of the simulated PM_{10} concentrations are also in reasonably good agreement with the

measurements in Tehran. The model captures the diurnal cycle and the magnitude of observed PM_{10} mass concentrations during most of the both simulation periods. The occurrence of the late night minimum of the observed hourly PM_{10} mass in May period was not predicted in the model. This error arises very likely from using a constant rate for the aerosol emissions throughout the simulation period. The consideration of a temporal better resolved emission rate for each aerosol components can improve the local behavior of aerosol mass. There is a difference between the amount of observed and simulated PM_{10} concentration on 11 May and 28 February, presumably because of the large underestimation of precipitation by the model.

The inclusion of aerosols feedback in shortwave radiation scheme, improved the simulated daily mean shortwave radiation flux in Tehran in both simulation periods. The errors in simulated shortwave radiation resulted mostly from limitation of the model in simulating clouds and precipitation. The other factors that might contribute to the differences between the simulations and observations are the uncertainties in simulating wind speed and direction and other meteorological fields. Quantifying the relative contribution of meteorological and chemical uncertainties on the predicted concentration of particulates is the subject of next studies.

Aerosol models as developed for this study are necessary tools to identify sources of air pollution and to develop mitigation strategies. The study has shown that mineral dust contributes most to the aerosol loading. The dominating contribution of natural aerosols to the Tehran air pollution challenges also the PM_{10} concept as air pollution measure.

Acknowledgements. The authors wish to thank the Max Planck Institute for Meteorology in Hamburg (MPI-M) for providing the HAM model codes and support for two stays of the first author at MPI-M.

The service charges for this open access publication have been covered by the Max Planck Society.

References

Ackermann, I. J., Hass, H., Memmesheimer, M., Ebel, E., Binkowski, F. S., and Shankar, U.: Modal aerosol dynamics model for Europe: Development and first applications, Atmos. Environ., 32, 2981–2999, 1998.

Albrecht, B. A.: Aerosols, cloud microphysics, and fractional cloudiness, Science, 245, 1227–1230, 1989.

Barnard, J. C., Chapman, E. G., Fast, J. D., Schemlzer, J. R., Slusser, J. R., and Shetter, R. E.: An evaluation of the FAST–J photolysis algorithm for predicting Nitrogen Dioxide photolysis rates under clear and cloudy sky conditions, Atmos, Environ., 38, 3393–3403, 2004a.

Chang, J. S., Binkowski, F. S., Seaman, N. L., McHenry, J. N., Samson, P. J., Stockwell, W. R., Walcek, C. J., Madornich, S., Middleton, P. B., Pleim, J. E., and Lansford, H. H.: The regional acid deposition model and engineering model, state-of-science/Technology, Report 4, National Acid Precipitation Assessment Program, Washington DC, 1989.

Charlson, R. J., Lovelock, J. E., Andreae, M. O., and Warren, S. G.: Oceanic phytoplankton, atmospheric sulfur, cloud albedo and climate, Nature, 326, 655–661, 1987.

Charlson, R. J., Schwartz, S. E., Hales, J. M., Cess, R. D., Coakley Jr., J. A., Hansen, J. E., and Hofmann, D. J.: Climate forcing by anthropogenic aerosols, Science, 255, 423–430, 1992.

Chou, M. D., Suarez, M. J., Ho, C. H., Yan, M. H. H., and Lee, K. T.: Parameterizations for cloud overlapping and shortwave single-scattering properties for use in general circulation and cloud ensemble models, J. Climate, 11, 202–214, 1998.

Dentener, F., Kinne, S., Bond, T., Boucher, O., Cofala, J., Generoso, S., Ginoux, P., Gong, S., Hoelzmann, J. J., Ito, A., Marelli, L., Penner, J. E., Putaud, J. P., Textor, C., Schulz, M., Van der Werf, J. R., and Wilson, J.: Emissions of primary aerosol and precursor gases

in the years 2000 and 1750 orescribed data-sets for AeroCom, J. Atmos. Chem. Phys., 6, 4321–4344, 2006, http://www.atmos-chem-phys.net/6/4321/2006/.
Fast, J. D., Gustafson, W. I., Easter Jr., R. C., Zaveri, R. A., Barnard, J. C., Chapman, E. G., Grell, G. A., and Peckham, S. E.: Evolution of ozone, particulates, and aerosol direct radiative forcing in the vicinity of Houston using a fully coupled meteorology-chemistry-aerosol model, J. Geophys. Res., 111, D21305, doi:10.1029/2005JD006721, 2006.
Fuchs, N. A.: Evaporation and Droplet Growth in Gaseous Media, Pergamon, Tarrytown, New York, 72 pp., 1959.
Fuchs, N. A.: The Mechanics of Aerosols, Pergamon press, Oxford, 1964.
Gong, S. L., Barriel, A., and Lazare, M.: Canadanian Aerosol Module: A size-segregated simulation of atmospheric aerosol processes for climate and air quality models: 1. Module development, J. Geophys. Res., 108(D1), 4007, doi:10.1029/2001JD002002, 2003.
Grell, G. A. and Devenyi, D.: A generalized approach to parameterizing convection combining ensemble and data assimilation techniques, Geophys. Res. Lett., 29(14), 38.1–38.4 2002.
Grell, G. A., Peckham, S. E., Schmitz, R., McKeen, S. A., Frost, G., Skamarock, W. C., and Eder, B.: Fully coupled "online" chemistry within the WRF model, Atmos. Environ., 39, 6957–6975, 2005.
Hong, S. Y., Noh, Y., and Dudhia, J.: A new vertical diffusion package with an explicit treatment of entrainment processes, Mon. Weather Rev., 134, 2318–2341, 2006.
IPCC, Climate Change 2007 – The Physical Science Basis, contribution of the Working Group I to the forth assessment Report of the Intergovernmental Panel on Climate Change, edited by: Solomon, S., Qin, D., Manning, M., Chen, Z., Marquis, K. B., Tignor, M., and Miller, H. L., Cambridge Univ. Press, Cambridge, United Kingdom and New York, NY, USA, 2007.
Jacobson, M. Z.: Global direct radiative forcing due to muticomponent anthropogenic and natural aerosols, J. Geophys. Res., 106, 1551–1568, 2001.
Kulmala, M., Laaksonen, A., and Pirjola, L.: Parameterizations for sulfuric acid/water nucleation rates, J. Geophys. Res., 103, 8301–8307, 1998.
Mlawer, E. J., Taubman, S. J., Brown, P. D., Iacono, M. J., and Clough, S. A.: Radiative transfer for inhomogeneous atmosphere: RRTM, a validated correlated-K model for longwave, J. Geophys. Res., 102, 16 663–16 682, 1997.
Monin, A. S. and Obukhov, A. M.: Basic laws of turbulent mixing in the ground layer of the atmosphere, Trans. Geophys. Inst. Akad. Nauk USSR, 151, 163–187, 1954.

Pleim, J. E., Venkatram, A., and Yamartino, R.: ADOM/TADAP Model Development Program, Vol. 4, The Dry Deposition Module, Ontario Ministry of the Environment, Canada, 1984.
Ramanathan, V. and Vogelmann, A. M.: Greenhouse effect, atmospheric solar absorption, and the Earth's radiation budget: From the Arrhenius-Langely era to the 1990's, Ambio, 26(1), 38–46, 1997.
Ramanathan, V., Crutzen, P. J., Kiehl, J. T., and Rosenfeld, D.: Aerosols, climate, and the hydrological cycle, Science, 294, 2119–2124, 2001a.
Ramanathan, V.: Indian Ocean Exprement: An integrated analysis of the climate forcing and effects of the great Indo-Asian haze, J. Geophys, Res., 106, 28 371–28 398, 2001b.
Rodriguez, M. A. and Dabdub, D.: IMAGES-SCAPE2: A modeling study of size- and chemistry resolved aerosol thermodynamics in a global chemical transport model, J. Geophys. Res., 109, D02203, doi:10.1029/2003JD003639, 2004.
Schell B., Ackermann, I. J., Hass, H., Binkowski, F. S., and Ebel, A.: Modeling the formation of secondary organic aerosol within a comprehensive air quality model system, J. Geophys. Res., 106, 28 275–28 293, 2001.
Skamarock, W. C., Klemp, J. B., Dudhia, J., Gill, D. O., Barker, D. M., Wang, W., and Powers, J. G.: A description of the Advanced Research WRF version 2, NCAR Tech Note, NCAR/TN468+STR, 88 pp., 2005.
Slinn, S. A. and Slinn, W. G. N.: Predictions for particle deposition on natural waters, Atmos. Environ., 14, 1013–1016, 1980.
Stier, P., Feichter, J., Kinne, S., Kloster, S., Vignati, E., Wilson, J., Ganzeveld, L., Tegen, I., Werner, M., Balkanski, Y., Schulz, M., Boucher, O., Minikin, A., and Petzold, A.: The aerosol-climate model ECHAM5-HAM, Atmos. Chem. Phys., 5, 1125–1156, 2005, http://www.atmos-chem-phys.net/5/1125/2005/.
Twomey, S.: Aerosols, clouds and radiation, Atmos. Environ. A-Gen., 25, 2435–2442, 1991.
Vehkamaki, H., Kulmala, M., Napari, I., Lehtinen, K. E. J., Timmreck, C., Noppel, M., and Laaksonen, A.: An improved parameterization for sulfuric acid-water nucleation rates for tropospheric and stratospheric conditions, J. Geophys. Res., 107(D22), 4622, doi:10.1029/2002JD002184, 2002.
Vignati, E., Wilson, J., and Stier, P.: M7: a size resolved aerosol mixture module for the use in global aerosol models, J. Geophys. Res., 109, D22202, doi:10.1029/2003JD004485, 2004.
Whitby, E. R. and McMurry, P. H.: Modal aerosol dynamics modeling, Aerosol Sci. Technol., 27, 673–688, 1997.

Wild, O., Zhu, X., and Prather, M. J.: Fast-J: Accurate simulation of in- and bellow-cloud photolysis in tropospheric chemical models, J. Atmos. Chem., 37, 245–282, 2000.

Williams, M. M. R., and Loyalka, S. K.: Aerosol Science: Theory and Practice, Pergamon, New York, 1991.

Wilson, J., Cuvelier, C., and Raes, F.: A modeling study of global mixed aerosol fields, J. Geophys. Res., 106, 34 081–34 108, 2001.

Wesely, M. L.: Parameterization of surface resistance to gaseous dry deposition in regional numerical models, Atmos. Environ., 16, 1293–1304, 1989.

Zaveri, R. A., Easter, R. C., and Wexler, A. S.: A new method for multicomponent activity coefficients of electrolytes in aqueous atmospheric aerosols, J. Geophys. Res., 110, D02201, doi:10.1029/2004JD004681, 2005a.

Zaveri, R. A., Easter, R. C., and Peters, L. K.: A computationally efficient Multicomponent Equilibrium Solver for Aerosols (MESA), J. Geophys. Res., 110, D24203, doi:10.1029/2004JD005618, 2005b.

Table 1. The modal structure of HAM model. N_i denotes the total aerosol number of the mode i and M_i^j denotes the mass of compound $j \in \{\mathrm{SU}, \mathrm{BC}, \mathrm{POM}, \mathrm{SS}, \mathrm{DU}\}$ in mode.

Modes	Soluble/Mixed	Insoluble
Nucleation ($\bar{r} \leq 0.005$)	N_1, M_1^{SU}	
Aitken ($0.005 < \bar{r} \leq 0.05$)	N_2, M_2^{SU}, M_2^{BC}, M_2^{POM}	N_5, M_5^{BC}, M_5^{POM}
Accumulation ($0.05 < \bar{r} \leq 0.5$)	N_3, M_3^{SU}, M_3^{BC}, M_3^{POM}, M_3^{SS}, M_3^{DU}	N_6, M_6^{DU}
Coarse ($\bar{r} > 0.5$)	N_4, M_4^{SU}, M_4^{BC}, M_4^{POM}, M_4^{SS}, M_4^{DU}	N_7, M_7^{DU}

GMDD
2, 681–707, 2009

Table 2. Prescribed scavenging parameter R for the modes of HAM model.

Mode	R
Nucleation soluble	0.20
Aitken soluble	0.60
Accumulation soluble	0.99
Coarse soluble	0.99
Aitken insoluble	0.20
Accumulation insoluble	0.40
Coarse insoluble	0.40

Table 3. Configuration options employed by WRF-chem in this study.

Atmospheric process	Model 0ption	Reference
Longwave radiation	RRTM	Mlawer et al. (1997)
Shortwave radiation	Goddard	Chou et al. (1998)
Surface layer	Monin-Obokhov	Monin and Obokhov (1954)
Land surface	Thermal diffusion	Skamarock et al. (2005)
Boundary layer	YSU	Hong et al. (2006)
Cumulus clouds	Grell-Devenyi	Grell and Devenyi (2002)
Cloud microphysics	Turned off	–
Gas-phase chemistry	RADM2	Chang et al. (1989)
Aerosol chemistry	HAM	Stier et al. (2005)
Photolysis	Fast-J	Wild et al. (2000), Barnard et al. (2004a)

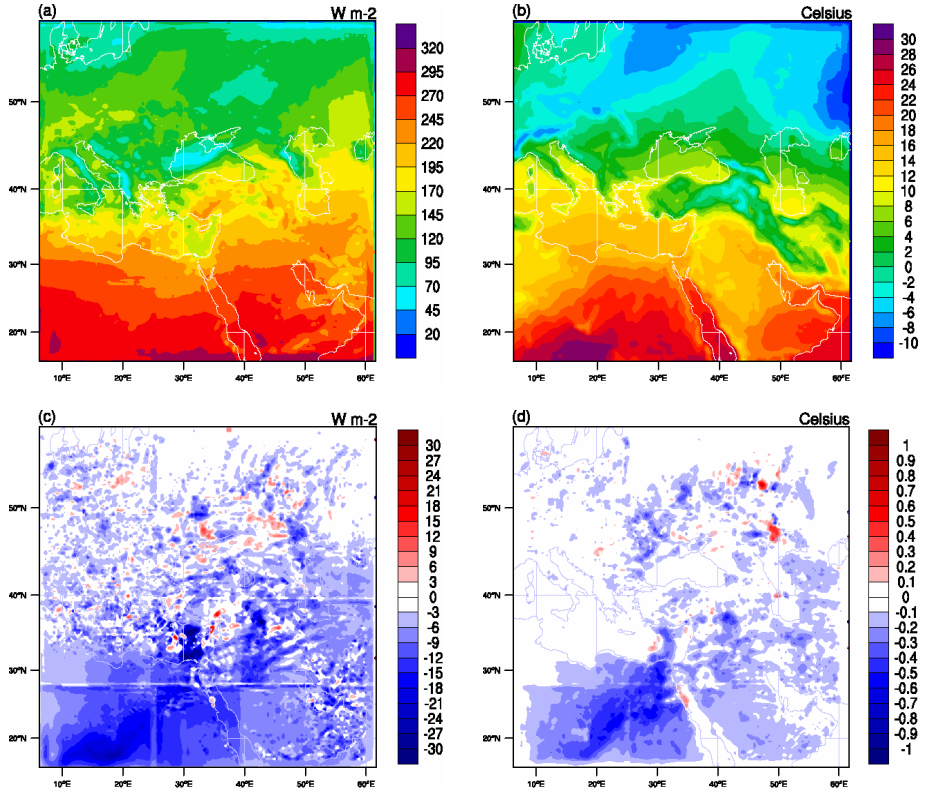

Fig. 1. Simulated **(a)** mean incident shortwave radiation, **(b)** mean surface temperature by WRF-HAM model for the 6-day period in February. Difference in simulated mean **(c)** shortwave radiation and **(d)** temperature with and without aerosols for the same period.

GMDD
2, 681–707, 2009

HAM model within WRF modeling system

R. Mashayekhi et al.

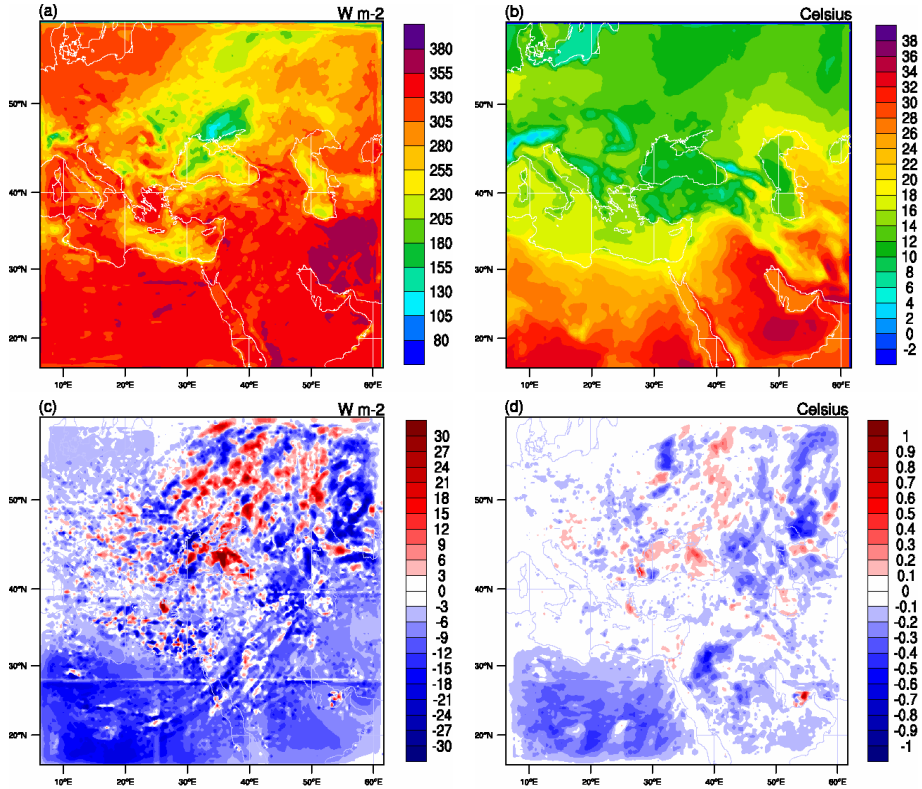

Fig. 2. Same as Fig. 1 except for the simulation period in May.

GMDD

2, 681–707, 2009

HAM model within WRF modeling system

R. Mashayekhi et al.

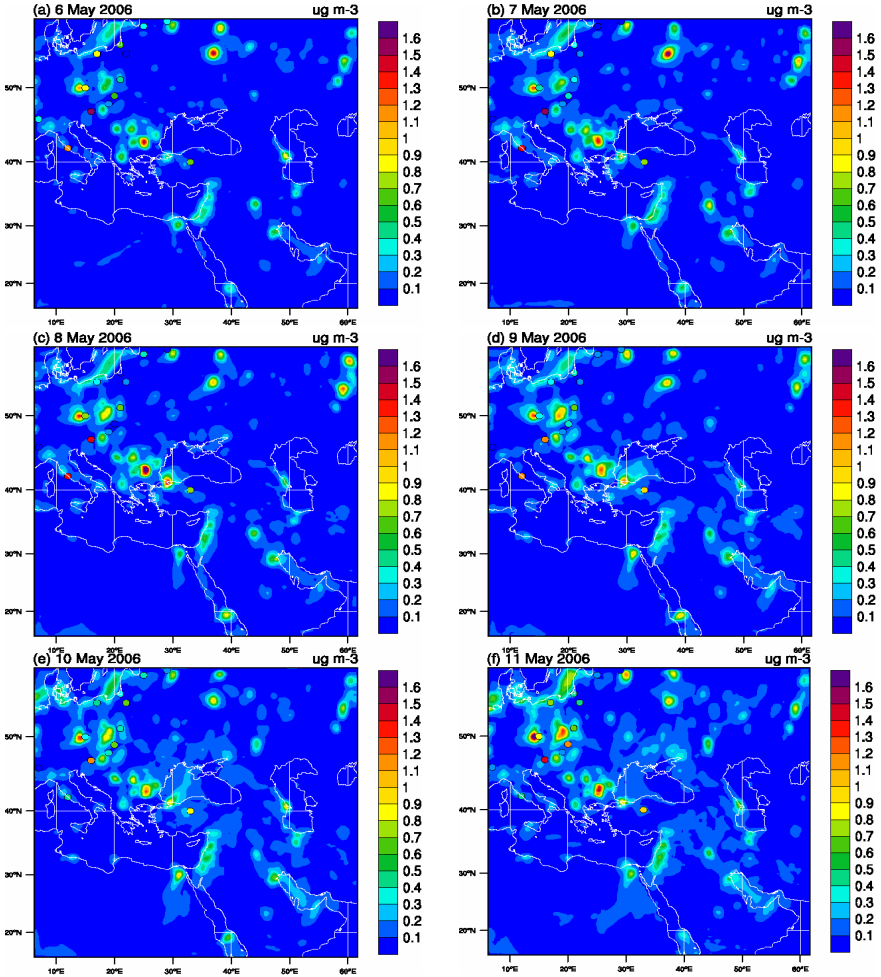

Fig. 3. The spatial distribution of the simulated and observed (colored circle) daily mean sulfate mass concentration on **(a)** 6 May, **(b)** 7 May, **(c)** 8 May, **(d)** 9 May, **(e)** 10 May, and **(f)** 11 May 2006.

GMDD
2, 681–707, 2009

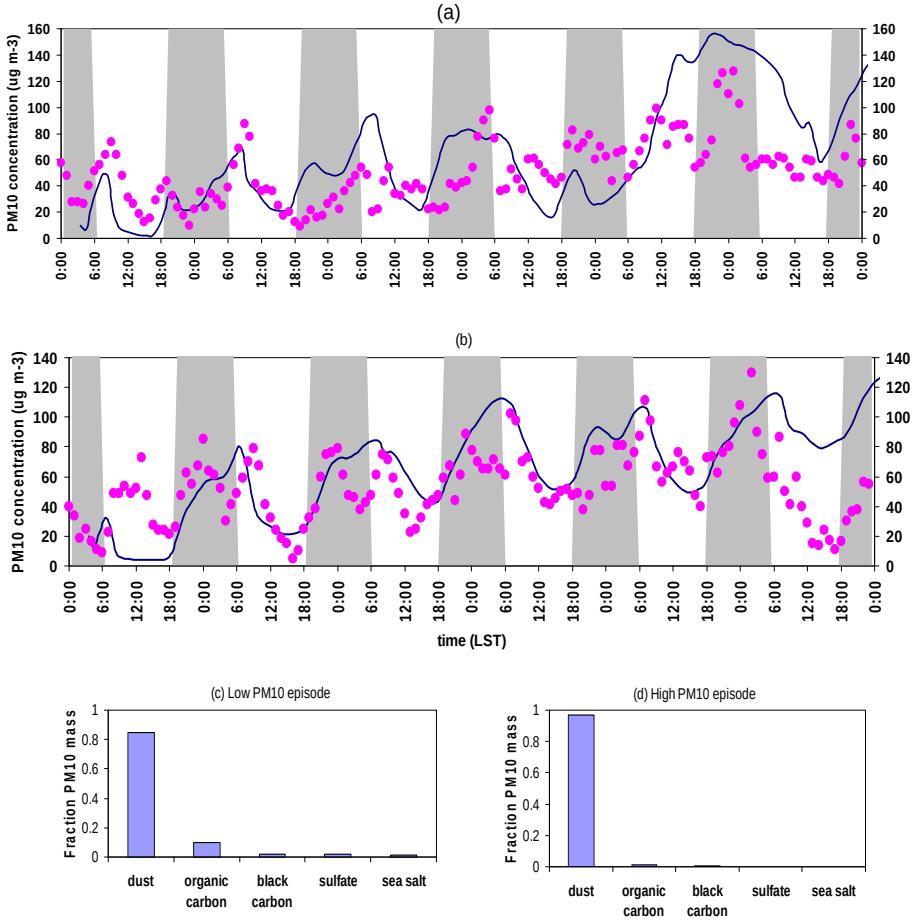

Fig. 4. Time series of observed (dots) and simulated (line) PM_{10} in Tehran during the simulation periods from **(a)** 22 to 28 February 2006 and **(b)** 6 to 12 May 2006. The model predicted PM_{10} composition (bottom panels) averaged over the selected **(c)** low and **(d)** high PM_{10} episode.

GMDD
2, 681–707, 2009

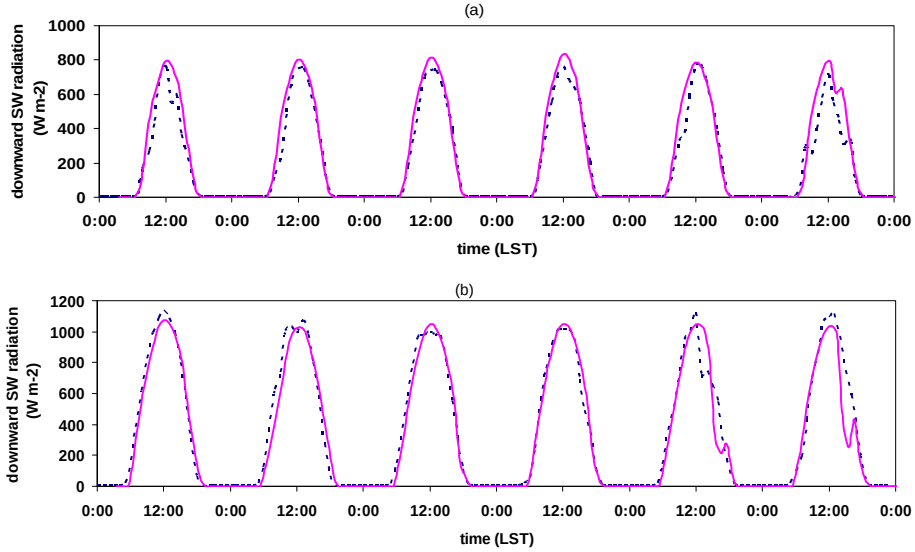

Fig. 5. Simulated (line) and observed (dashed line) downward shortwave radiation flux in Tehran during the time between the episode **(a)** 22 to 28 February, and **(b)** 6 to 12 May 2006.

GMDD
2, 681–707, 2009

HAM model within WRF modeling system

R. Mashayekhi et al.

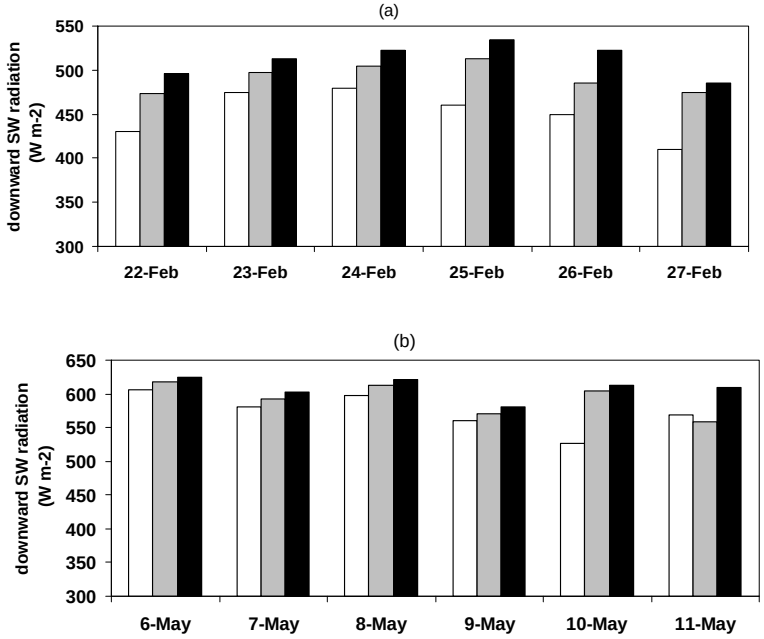

Fig. 6. Observed (white column) daily mean downward shortwave radiation and the simulations with (gray column) and without (black column) the aerosol feedback during the time between the episode **(a)** 22 to 28 February 2006 **(b)** 6 to 12 May 2006 in Tehran.

GMDD
2, 681–707, 2009